\



Instantaneous frequency measurement using two parallel I/Q modulators based on optical power monitoring

Chuangye Wang(王创业), Tigang Ning(宁提纲), Jing Li(李晶), Li Pei(裴丽), Jingjing Zheng(郑晶晶), and Jingchuan Zhang(张景川)

Citation: Chin. Phys. B, 2022, 31 (**1**): 010702. DOI: 10.1088/1674-1056/ac1923
Journal homepage: http://cpb.iphy.ac.cn; http://iopscience.iop.org/cpb

What follows is a list of articles you may be interested in

Optical state selection process with optical pumping in a cesium atomic fountain clock

Lei Han(韩蕾), Fang Fang(房芳), Wei-Liang Chen(陈伟亮), Kun Liu(刘昆), Ya-Ni Zuo(左娅妮), Fa-Song Zheng(郑发松), Shao-Yang Dai(戴少阳), and Tian-Chu Li(李天初)
Chin. Phys. B, 2021, 30 (**8**): 080602. DOI: 10.1088/1674-1056/ac0698

Real-time frequency transfer system over ground-to-satellite link based on carrier-phase compensation at 10^{-16} level

Hui-Jian Liang(梁慧剑), Shi-Guang Wang(王时光), Yu Bai(白钰), Si-Chen Sun(孙思忱), and Li-Jun Wang(王力军)
Chin. Phys. B, 2021, 30 (**8**): 080601. DOI: 10.1088/1674-1056/ac05a6

Evaluation of second-order Zeeman frequency shift in NTSC-F2

Jun-Ru Shi(施俊如), Xin-Liang Wang(王心亮), Yang Bai(白杨), Fan Yang(杨帆), Yong Guan(管勇), Dan-Dan Liu(刘丹丹), Jun Ruan(阮军), and Shou-Gang Zhang(张首刚)
Chin. Phys. B, 2021, 30 (**7**): 070601. DOI: 10.1088/1674-1056/abe375

Improvement of the short-term stability of atomic fountain clock with state preparation by two-laser optical pumping

Lei Han(韩蕾), Fang Fang(房芳), Wei-Liang Chen(陈伟亮), Kun Liu(刘昆), Shao-Yang Dai(戴少阳), Ya-Ni Zuo(左娅妮), and Tian-Chu Li(李天初)
Chin. Phys. B, 2021, 30 (**5**): 050602. DOI: 10.1088/1674-1056/abe22a

Nb_5N_6 microbolometer array for terahertz detection

Tu Xue-Cou, Kang Lin, Liu Xin-Hua, Mao Qing-Kai, Wan Chao, Chen Jian, Jin Biao-Bing, Ji Zheng-Ming, Xu Wei-Wei, Wu Pei-Heng
Chin. Phys. B, 2013, 22 (**4**): 040701. DOI: 10.1088/1674-1056/22/4/040701

Instantaneous frequency measurement using two parallel I/Q modulators based on optical power monitoring

Chuangye Wang(王创业)[1], Tigang Ning(宁提纲)[1], Jing Li(李晶)[1,†], Li Pei(裴丽)[1], Jingjing Zheng(郑晶晶)[1], and Jingchuan Zhang(张景川)[2]

[1] *Key Laboratory of All Optical Network and Advanced Telecommunication Network of EMC, Institute of Lightwave Technology, Beijing Jiaotong University, Beijing* 100044, *China*
[2] *Beijing Institute of Spacecraft Environment Engineering, Beijing* 100029, *China*

(Received 30 April 2021; revised manuscript received 12 July 2021; accepted manuscript online 30 July 2021)

A scheme for instantaneous frequency measurement (IFM) using two parallel I/Q modulators based on optical power monitoring is proposed. The amplitude comparison function (ACF) can be constructed to establish the relationship between the frequency of radio frequency (RF) signal and the power ratio of two optical signals output by two I/Q modulators. The frequency of RF signal can be derived by measuring the optical power of the optical signals output by two I/Q modulators. The measurement range and measurement error can be adjusted by controlling the delay amount of the electrical delay line. The feasibility of the scheme is verified, and the corresponding measurement range and measurement error of the system under different delay amounts of the electrical delay line are given. Compared with previous IFM schemes, the structure of this scheme is simple. Polarization devices, a photodetector and an electrical power meter are not used, which reduces the impact of the environmental disturbance on the system and the cost of the system. In simulation, the measurement range can reach 0 GHz–24.5 GHz by adjusting the delay amount of the electrical delay line $\tau = 20$ ps. The measurement error of the scheme is better at low frequency, and the measurement error of low frequency 0 GHz–9.6 GHz can reach -0.1 GHz to $+0.05$ GHz.

Keywords: microwave photonics, instantaneous frequency measurement, optical power monitoring

PACS: 07.57.–c, 06.30.Ft, 06.20.Dk **DOI:** 10.1088/1674-1056/ac1923

1. Introduction

Instantaneous frequency measurement (IFM) has been a research hotspot in recent years. It has important applications in both military and civil fields, such as radar, communication systems, and electronic warfare systems.[1,2] The traditional electronics method is no longer suitable for future development due to the disadvantages of large loss, small measurement bandwidth and no immunity to electromagnetic interference, but the photonics method perfectly overcomes these shortcomings.[3–5] The researchers have proposed many IFM schemes based on photonics methods, for example, based on the frequency-space mapping method,[6–8] frequency-time mapping method,[9–14] frequency-phase mapping method,[15,16] and frequency-power mapping method. Among them, the method based on frequency-power mapping is the most common. The basic principle is to use a modulator to modulate the received RF signal, then the modulated signal is divided into two channel signals and processed in the optical domain, and the processed optical signals are directly used to measure the optical power, or converted into electrical signals by the photodetector to measure the electrical power. The ACF is constructed to establish the corresponding relationship between the frequency of the RF signal and the power ratio of two channel signals. The frequency of the RF signal can be determined by monitoring the optical power ratio or the electrical power ratio of the two channel signals. In Refs. [17–20], these schemes first used a modulator to modulate the input RF signal, then the modulated signal went through different dispersion processes to achieve different power attenuation, and finally a fixed relationship between the input RF frequency and the power ratio of two output signals was established. The frequency of the RF signal can be derived from the power ratio. In Refs. [21,22], the input RF signal first entered Mach–Zehnder modulator (MZM) for carrier suppression modulation, then the optical filter was used to process the modulated signal, and finally the power ratio of the two processed signals was used to derive the frequency of the input RF signal. In Ref. [23], a phase modulator was put into a Sagnac loop to establish a relationship between the amplitude of the direct current output and the input RF frequency. The measurement range can reach 0.01 GHz–40 GHz and the measurement error is less than 6%. In addition, IFM can also be realized by converting frequency information into power information based on stimulated Brillouin scattering,[24,25] resonators,[26,27] and four-wave mixing.[28] Although these schemes can realize IFM, they are relatively complex in structure. In Ref. [29], the author realized IFM based on a dual-polarization modulator and an electrical delay line. Compared with the previous IFM schemes, the structure is simpler and the cost is lower (there is no expensive high-

[†]Corresponding author. E-mail: lijing@bjtu.edu.cn

© 2022 Chinese Physical Society and IOP Publishing Ltd

speed electronic device). However, in this scheme, the polarization controller needs to be accurately kept at 45°, which increases the instability of the system (the polarization device is sensitive to the environment).

In this paper, a simpler structure for IFM is proposed. The scheme only uses one optical source, one electrical delay line, two I/Q modulators and two optical power meters. By setting the bias point of two I/Q modulators appropriately, a fixed relationship between the input signal frequency and the power ratio of two optical signals output by two I/Q modulators is established. The input signal frequency can be derived by the power ratio. The measurement range and measurement error can be adjusted by changing the delay amount of the electrical delay line. The scheme has a better measurement error for low frequency compared with other schemes. The measurement error of low frequency 0 GHz–9.6 GHz can reach −0.1 GHz to +0.05 GHz in simulation.

2. Model and theoretical analysis

Figure 1 shows the schematic diagram of the proposed scheme. The optical signal generated by the CW laser is first divided into two equal power optical signals by an optical power splitter. The two equal power optical signals are injected into two I/Q modulators respectively. I/Q modulator 1 consists of two sub-modulators (MZM-1 and MZM-2), and I/Q modulator 2 consists of two sub-modulators (MZM-3 and MZM-4). The RF signal generated by the RF source is first divided into two equal power electrical signals by an electrical power splitter. One channel electrical signal first passes through an electrical delay line and then is divided by an electrical power splitter, and the generated two electrical signals are injected into the input RF ports of MZM-1 and MZM-3 respectively. The other channel electrical signal passes through an electrical power splitter and the generated two electrical signals are injected into the RF input ports of MZM-2 and MZM-4 respectively. MZM-1, MZM-2, MZM-3 and MZM-4 are biased at minimum transmission point (MITP). I/Q modulator 1 and I/Q modulator 2 are biased at maximum transmission point (MATP) and MITP respectively. Suppose the phase shift induced by DC bias of MZM-1, MZM-2, MZM-3, MZM-4, I/Q modulator 1 and I/Q modulator 2 are ϕ_1, ϕ_2, ϕ_3, ϕ_4, ϕ_5, and ϕ_6 respectively, so $\phi_1=\phi_2=\phi_3=\phi_4=\phi_6=\pi$ and $\phi_5=0$. The output optical signal by CW laser is $E_{\text{in}}(t)=E_0\exp(\text{j}\omega_0 t)$, where E_0 and ω_0 denote the amplitude and angular frequency respectively. The output electrical signal by the RF source is $V_{\text{RF}}(t)=V_{\text{RF}}\cos(\Omega t)$, where V_{RF} and Ω denote the amplitude and angular frequency respectively. The delay amount of the electrical delay line is τ. The output optical signal of I/Q modulator 1 and I/Q modulator 2 can be expressed as

$$\begin{aligned}E_1 &= \frac{1}{2}E_{\text{in}}(t)\exp\left(\text{j}\frac{\pi}{2}\right)\\ &\quad\times\{\sin[m\cos(\Omega t+\Omega\tau)]+\sin[m\cos(\Omega t)]\},\\ E_2 &= \frac{1}{2}E_{\text{in}}(t)\exp\left(\text{j}\frac{\pi}{2}\right)\\ &\quad\times\{\sin[m\cos(\Omega t+\Omega\tau)]-\sin[m\cos(\Omega t)]\},\end{aligned}\tag{1}$$

where m denotes the modulation index of MZM and $m=\pi V_{\text{RF}}/\left(2\sqrt{2}V_\pi\right)$. V_π denotes the half-wave voltage of MZM.

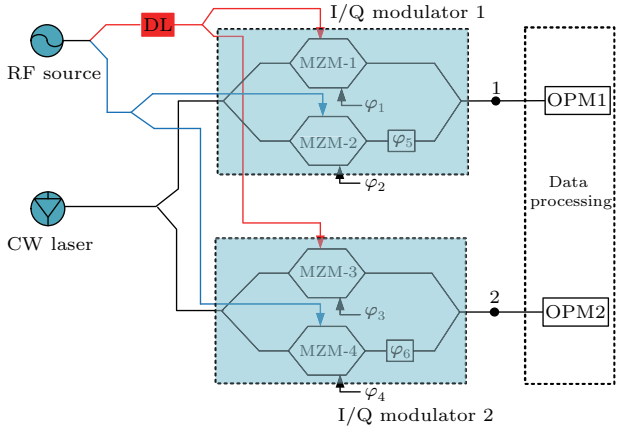


Fig. 1. The schematic diagram of the scheme (RF source: radio frequency source; CW laser: continuous-wave laser; MZM: Mach–Zehnder modulator; DL: electrical delay line; OPM: optical power meter; ϕ_1, ϕ_2, ϕ_3, ϕ_4, ϕ_5, and ϕ_6: phase shifts induced by the DC bias of MZM-1, MZM-2, MZM-3, MZM-4, I/Q modulator 1, and I/Q modulator 2, respectively).

Use Jacobi–Anger expansion to expand Eq. (1)

$$\begin{aligned}E_1 &= a_n\cos\left[(2n-1)\left(\Omega t+\frac{\Omega\tau}{2}\right)\right],\\ E_2 &= b_n\sin\left[(2n-1)\left(\Omega t+\frac{\Omega\tau}{2}\right)\right],\end{aligned}\tag{2}$$

where

$$\begin{aligned}a_n &= -2E_{\text{in}}(t)\exp\left(\text{j}\frac{\pi}{2}\right)\\ &\quad\times\sum_{n=1}^{\infty}(-1)^n J_{2n-1}(m)\cos\left[(2n-1)\frac{\Omega\tau}{2}\right],\\ b_n &= 2E_{\text{in}}(t)\exp\left(\text{j}\frac{\pi}{2}\right)\\ &\quad\times\sum_{n=1}^{\infty}(-1)^n J_{2n-1}(m)\sin\left[(2n-1)\frac{\Omega\tau}{2}\right],\end{aligned}\tag{3}$$

Here, $J_n(\cdot)$ represents the Bessel function of the first kind of order n. Since the received signal is weak, the scheme can only consider the first-order sidebands, and Eq. (2) can be simplified as

$$\begin{aligned}E_1 &= 2E_{\text{in}}(t)\exp\left(\text{j}\frac{\pi}{2}\right)\\ &\quad\times J_1(m)\cos\left[\frac{\Omega\tau}{2}\right]\cos\left(\Omega t+\frac{\Omega\tau}{2}\right),\\ E_2 &= -2E_{\text{in}}(t)\exp\left(\text{j}\frac{\pi}{2}\right)\\ &\quad\times J_1(m)\sin\left[\frac{\Omega\tau}{2}\right]\sin\left(\Omega t+\frac{\Omega\tau}{2}\right).\end{aligned}\tag{4}$$

The optical intensity of signals output by I/Q modulator 1 and I/Q modulation 2 are

$$I_1 = 4E_0^2 J_1^2(m)\cos^2\left(\frac{\Omega\tau}{2}\right),$$
$$I_2 = 4E_0^2 J_1^2(m)\sin^2\left(\frac{\Omega\tau}{2}\right). \quad (5)$$

ACF is defined as the power ratio of optical signals output by two I/Q modulators, and the ACF can be expressed as

$$\mathrm{ACF} = \frac{P_1}{P_2} = \frac{1}{\tan^2(\Omega\tau/2)} = \frac{1}{\tan^2(\pi\tau f)}, \quad (6)$$

where f denotes the frequency of the received RF signal.

According to Eq. (6), when τ is a fixed value, there is a one-to-one corresponding relationship between f and P_1/P_2. Therefore, the frequency of the received RF signal can be derived by the power ratio of two optical signals generated by two I/Q modulators.

Figure 2 is calculated ACF, P_1, P_2 versus RF frequency diagram when $\tau = 20$ ps. Figure 3 is the ACF curve diagram corresponding $\tau = 20$ ps, 30 ps, 40 ps, and 50 ps. As can be seen in Fig. 3, different delay amount τ corresponds to different ACF curve. Different ACF curve determines different measurement range.

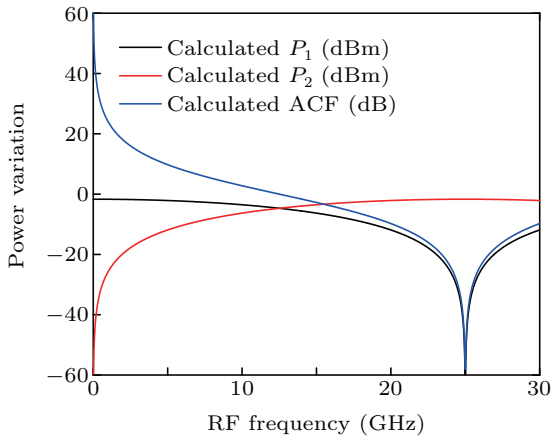


Fig. 2. Calculated ACF, calculated P_1, calculated P_2 versus RF frequency when $\tau = 20$ ps.

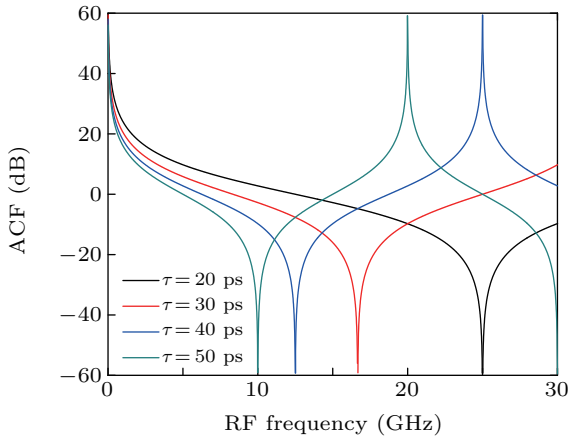


Fig. 3. Calculated ACF versus RF frequency when $\tau = 20$ ps, 30 ps, 40 ps, and 50 ps.

3. Simulation and discussion

The feasibility of the scheme is verified by simulation in the software OptiSystem. The parameters are set as follows: the power, wavelength and linewidth of the CW laser are 10 dBm, 1550.12 nm, and 10 MHz respectively. The extinction ratio, insertion loss and half-wave voltage of the MZM are 30 dB, 5 dB, and 4 V respectively. The amplitude of the RF source is 3.6 V (the modulation index of MZM is equal to 1). The electrical delay amount of the electrical delay line is 20 ps. MZM-1, MZM-2, MZM-3 and MZM-4 are biased at MITP. I/Q modulator 1 and I/Q modulator 2 are biased at MATP and MITP respectively. Figure 4 shows simulated received optical power values of the optical power meter 1 and optical power meter 2, and ACF curve when the frequency of RF changes from 0 GHz–30 GHz. As can be seen in Fig. 4, when the frequency of the input RF is from 0 GHz to 25 GHz, the ACF curve is monotonous. There is a one-to-one corresponding relationship between the frequency of the input RF and the value of ACF curve, so we can figure out the frequency of the input RF by the value of ACF in real time.

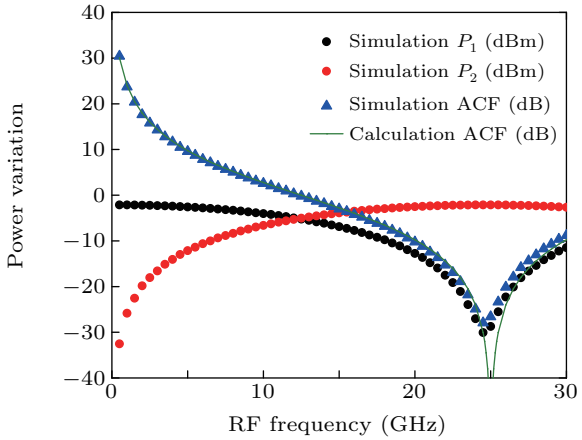


Fig. 4. Simulated ACF versus RF frequency when $\tau = 20$ ps.

In previous theoretical calculation, the extinction ratio of the modulator is considered to be infinite, but the extinction ratio of the MZM is finite in practice. The effect of extinction ratio of the MZM on the scheme needs to be considered. The extinction ratio of the MZM is set to 20 dB, 25 dB, and 30 dB respectively in the OptiSystem. The settings of other parameters remain unchanged. The relationship diagram between ACF and the input RF frequency can be obtained as shown in Fig. 5. Figure 5 shows that the higher the extinction ratio of the MZM is, the closer the obtained ACF curve is to the theoretical ACF curve. This is because the MZM cannot suppress the carrier and even-order sidebands effectively when the extinction ratio of the MZM is not high.

The effect of the modulation index of the MZM on the scheme also needs to be considered. The modulation index of the MZM is set to 0.5, 1.0, and 1.5 respectively. The extinction

ratio of the MZM is set to 30 dB. Other parameter settings remain unchanged. The relationship diagram between the ACF and the input RF frequency can be obtained as shown in Fig. 6. Figure 6 indicates that the larger the modulation index m is in a certain range, the closer the ACF curve is to the theoretical curve. This is because the amplitude difference between generated first-order optical sidebands and generated higher odd-order optical sidebands by the MZM will increase when the modulation index m increases in a certain range, which will reduce the effect of higher odd-order sidebands on the scheme. However, the ACF curves under different modulation index are only different at the end of the monotone interval (0 GHz–25 GHz) and most regions of the monotone interval coincide with the theoretical ACF curve, which indicates that this scheme is not required for the power of the input RF.

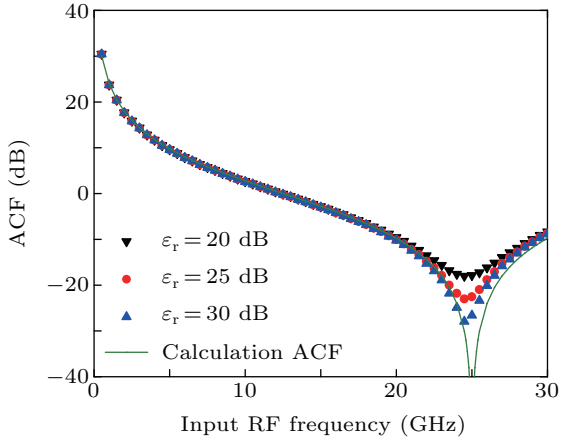


Fig. 5. Simulated ACF curve versus input RF frequency when $\varepsilon_r = 20$ dB, 25 dB, and 30 dB.

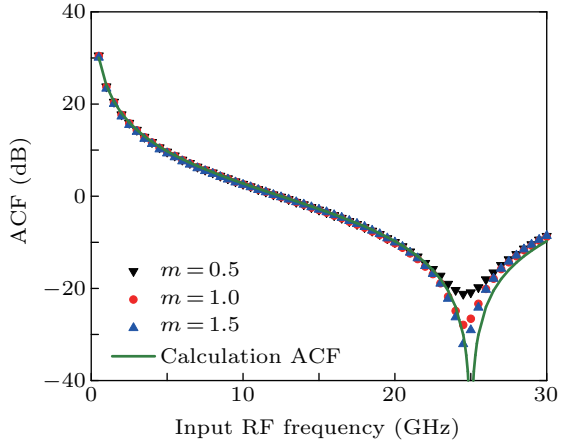


Fig. 6. Simulated ACF curve versus input RF frequency when $m = 0.5$, 1.0, and 1.5.

When the modulation index $m = 1$, the delay amount $\tau = 20$ ps and the extinction ratio of the MZM is 30 dB, the estimation error can be obtained as shown in Figs. 7(a) and 7(b). As shown in Fig. 7(a), the simulated frequency measurement results are approximately equal to the calculated frequency measurement results except around 25 GHz. The reason for the larger measurement error around 25 GHz is that the extinction ratio of the MZM is finite. As shown in Fig. 7(b), the estimation error is −0.15 GHz to +0.3 GHz in the measurement range of 0 GHz–24.5 GHz when $\tau = 20$ ps.

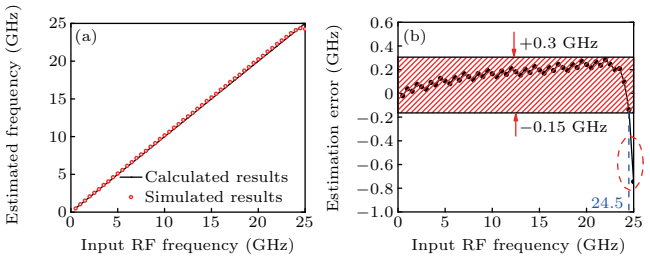


Fig. 7. (a) Estimated RF frequency versus input RF frequency. (b) Estimation error versus input RF frequency.

The estimation error is analyzed when $\tau = 30$ ps, 40 ps, and 50 ps. The simulated results are shown in Fig. 8. Figures 8(a) and 8(b) indicate that the measurement range and the measurement error are 0 GHz–16 GHz and −0.3 GHz to +0.05 GHz when $\tau = 30$ ps. The estimation error is larger around 16.7 GHz because the extinction ratio of MZM is finite. Similarly, it can be seen from Figs. 8(c) and 8(d) that the measurement range and measurement error are 0 GHz–12.2 GHz and −0.05 GHz to +0.2 GHz when $\tau = 40$ ps. Figures 8(e) and 8(f) indicate that the measurement range and measurement error are 0 GHz–9.6 GHz and −0.1 GHz to +0.05 GHz when $\tau = 50$ ps.

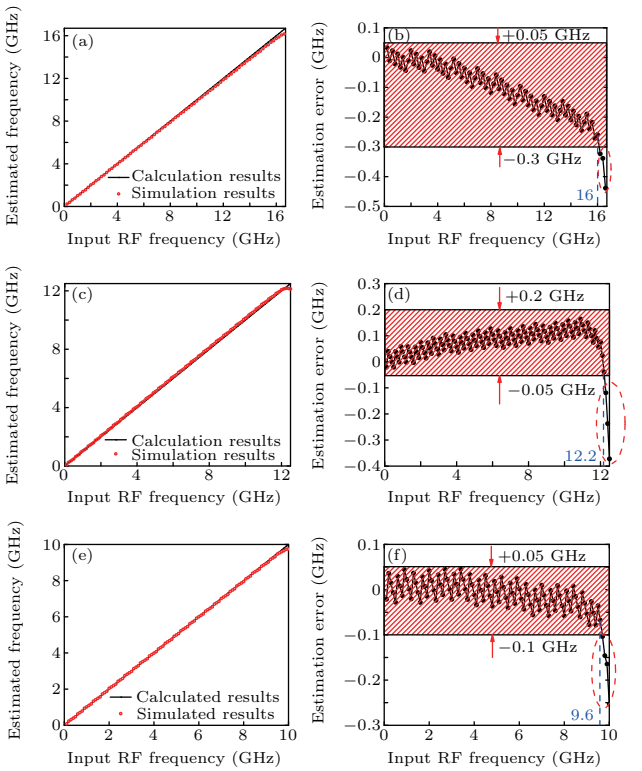


Fig. 8. Estimated RF frequency versus input RF frequency at different $\tau =$ (a) 30 ps, (c) 40 ps, (e) 50 ps. Estimation RF frequency error versus input RF frequency at different $\tau =$ (b) 30 ps, (d) 40 ps, (f) 50 ps.

Different measurement ranges and measurement errors are shown in Table 1. There is a trade-off balance between the measurement range and measurement error, as can be seen

in Table 1. When τ increases, the measurement range decreases, but the measurement error becomes better. Since the ACF curve in this scheme has a high slope at low frequency, the measurement error of low frequency is better than that of other schemes.

Table 1. Different measurement ranges and measurement errors.

Delay	Measurement range	Measurement error
$\tau = 20$ ps	0 GHz–24.5 GHz	−0.15 GHz to +0.3 GHz
$\tau = 30$ ps	0 GHz–16 GHz	−0.3 GHz to +0.05 GHz
$\tau = 40$ ps	0 GHz–12.2 GHz	−0.05 GHz to +0.2 GHz
$\tau = 50$ ps	0 GHz–9.6 GHz	−0.1 GHz to +0.05 GHz

In the scheme, the four sub-modulators are set as MITP. I/Q modulator 1 and I/Q modulator 2 are set as MATP and MITP respectively. The effect of DC bias drift of the MZM on the scheme needs to be considered. Suppose that $\Delta V/V_\pi$ is the DC bias drift of the MZM, where ΔV denotes the varied amount of DC bias voltage of the MZM and V_π denotes the half-wave voltage of the MZM. Take $\tau = 50$ ps for example. The DC bias drift of MZM-1, MZM-2, MZM-3, MZM-4, I/Q modulator 1 and I/Q modulator 2 are set to ±10% respectively. The corresponding parameter settings in the simulation software are shown in Table 2.

Table 2. Parameter settings for different modulators.

DC bias drift	DC bias voltage				Phase shift (φ_5 and φ_6)	
	MZM-1	MZM-2	MZM-3	MZM-4	I/Q modulator 1	I/Q modulator 2
−10%	3.6 V	3.6 V	3.6 V	3.6 V	−18°	162°
10%	4.4 V	4.4 V	4.4 V	4.4 V	18°	198°

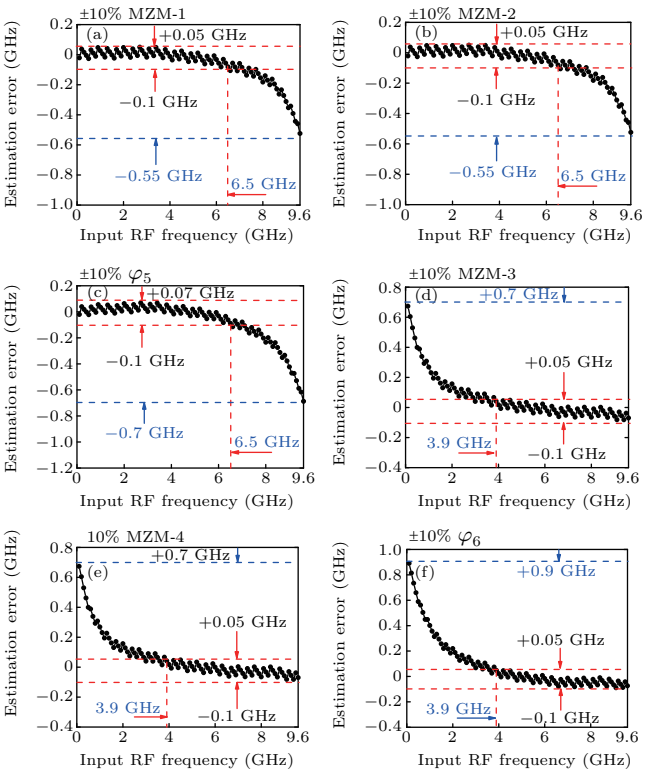


Fig. 9. Estimation error diagram when DC bias drift is ±10%: (a) MZM-1, (b) MZM-2, (c) I/Q modulator 1, (d) MZM-3, (e) MZM-4, (f) I/Q modulator 2.

Figures 9(a) and 9(b) are the estimation error diagrams when the DC bias drift of MZM-1 is ±10% and the DC bias drift of MZM-2 is ±10% respectively. As shown in Figs. 9(a) and 9(b), the estimation error becomes −0.55 GHz to +0.05 GHz. In order to reach the measurement error (−0.1 GHz to +0.05 GHz) before DC bias drift, the measurement range becomes 0 GHz–6.5 GHz. Figure 9(c) is the estimation error diagram when the DC bias drift of I/Q modulator 1 is ±10%. As shown in Fig. 9(c), the estimation error becomes −0.7 GHz to +0.07 GHz. In order to reach the measurement error −0.1 GHz to +0.07 GHz, the measurement range becomes 0 GHz–6.5 GHz.

Figures 9(d) and 9(e) are the estimation error diagrams when the DC bias drift of MZM-3 is ±10% and the DC bias drift of MZM-4 is ±10% respectively. As shown in Figs. 9(d) and 9(e), the estimation error becomes −0.1 GHz to +0.7 GHz. In order to reach the measurement error (−0.1 GHz to +0.05 GHz) before DC bias drift, the measurement range becomes 3.9 GHz–9.6 GHz. Figure 9(f) is the estimation error diagram when the DC bias drift of I/Q modulator 2 is ±10%. As shown in Fig. 9(f), the estimation error becomes −0.1 GHz to +0.9 GHz. In order to reach the measurement error (−0.1 GHz to +0.05 GHz) before DC bias drift, the measurement range becomes 3.9 GHz–9.6 GHz.

4. Conclusion

In this paper, a new scheme to realize IFM is proposed. The structure of the scheme is simple; it only consists of one optical source, one electrical delay line, two I/Q modulators, and two optical power meters. By setting each bias point of two I/Q modulators and the delay amount of the electrical delay line properly, a fixed relationship between the frequency of the RF signal and the optical power ratio can be obtained. Since the scheme is carried out in the optical domain, no expensive electronic devices are used. The scheme also has no polarization devices, which reduces the impact of environmental disturbances on the system. The measurement range and measurement error can be adjusted by changing the delay amount of the electrical delay line. Although there exists a trade-off balance between the measurement range and the measurement error, the measurement error of low frequency in

this scheme is better than other schemes because the slope of the ACF curve is large at the low frequency. The measurement error in low frequency 0 GHz–9.6 GHz can reach −0.1 GHz to +0.05 GHz. We believe this method will provide guidance for IFM in the future.

Acknowledgments

Project supported by the National Key Research and Development Program of China (Grant No. 2018YFB1801003), the National Natural Science Foundation of China (Grant Nos. 61525501 and 61827817), and the Beijing Natural Science Foundation, China (Grant No. 4192022).

References

[1] Ghelfi P, Laghezza F, Scotti F, Serafino G, Capria A, Pinna S, Onori D, Porzi C, Scaffardi M, Malacarne A, Vercesi V, Lazzeri E, Berizzi F and Bogoni A 2014 *Nature* **507** 341
[2] Spezio A 2002 *IEEE Transactions on Microwave Theory and Techniques* **50** 633
[3] Capmany J and Novak D 2007 *Nat. Photonics* **1** 319
[4] Yao J 2009 *J. Lightwave Technol.* **27** 314
[5] Seeds A and Williams K 2006 *J. Lightwave Technol.* **24** 4628
[6] Wang W, Davis R, Jung T, Lodenkamper R, Lembo L, Brock J and Wu M 2001 *IEEE Transactions on Microwave Theory and Techniques* **49** 1996
[7] Winnall S, Lindsay A, Austin M, Canning J and Mitchell A 2006 *IEEE Transactions on Microwave Theory and Techniques* **54** 868
[8] Wang L, Zhu N, Li W, Wang H, Zheng J and Liu J 2013 *Opt. Commun.* **286** 282
[9] Wang S, Wu G, Sun Y and Chen J 2019 *Opt. Express* **27** 25364
[10] Zhou F, Chen H, Wang X, Zhou L, Dong J and Zhang X 2018 *IEEE Photon. J.* **10** 1
[11] Liu J, Shi T and Chen Y 2021 *J. Lightwave Technol.* **39** 2023
[12] Hao T, Tang J, Li W, Zhu N and Li M 2018 *Opt. Express* **26** 33582
[13] Hao T, Tang J, Shi N, Li W, Zhu N and Li M 2019 *Opt. Lett.* **44** 3062
[14] Nguyen T, Chan E and Minasian R 2014 *Opt. Lett.* **39** 2419
[15] Shi J, Zhang F, Ben D and Pan S 2019 *IEEE Transactions on Microwave Theory and Techniques* **67** 544
[16] Zhu W, Sun J and Ge X 2015 *12th IEEE International Conference on Electronic Measurement & Instruments (ICEMI)*, July 16–18, 2015, p. 948
[17] Zhou J, Fu S, Shum P, Aditya S, Xia L, Li J, Sun X and Xu K 2009 *Opt. Express* **17** 7217
[18] Zhang X, Chi H, Zhang X, Zheng S, Jin X and Yao J 2009 *IEEE Microwave and Wireless Components Letters* **19** 422
[19] Li J, Ning T, Pei L, Jian W, Zheng J, You H, Chen H and Zhang C 2014 *Opt. Laser Technol.* **63** 54
[20] Zhang H and Pan S 2013 *Electron. Lett.* **49** 277
[21] Chi H, Zou X and Yao J 2008 *IEEE Photon. Technol. Lett.* **20** 1249
[22] Zou X, Chi H and Yao J 2009 *IEEE Transactions on Microwave Theory and Techniques* **57** 505
[23] Emami H, Hajihashemi M, Alavi S, Supaat A and Bui L 2018 *Opt. Lett.* **43** 2233
[24] Zou W, Long X, Li X, Xin G and Chen J 2019 *Opt. Lett.* **44** 2045
[25] Wang D, Pan L, Wang Y, Zhang Q, Du C, Wang K, Dong W and Zhang X 2019 *Opt. Laser Technol.* **113** 171
[26] Zhu B, Zhang W, Pan S and Yao J 2019 *J. Lightwave Technol.* **37** 2527
[27] Chen Y, Zhang W, Liu J and Yao J 2019 *Opt. Lett.* **44** 2402
[28] Pagani M, Morrison B, Zhang Y, Casas-Bedoya A, Aalto T, Harjanne M, Kapulainen M, Eggleton B and Marpaung D 2015 *Optica* **2** 751
[29] Li J, Pei L, Ning T and Zheng J 2020 *J. Lightwave Technol.* **38** 2285